

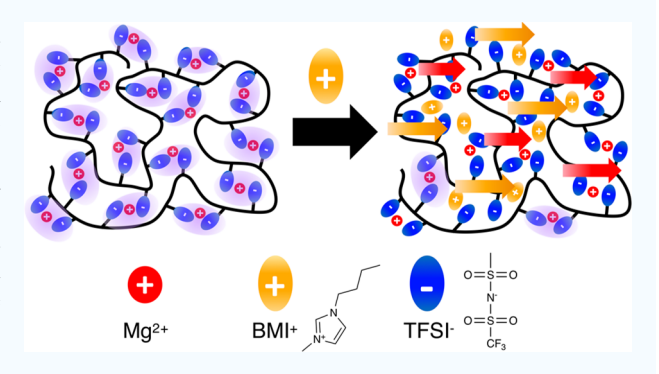
Dual Cation Exchanged Poly(ionic liquid)s as Magnesium **Conducting Electrolytes**

Bumjun Park, Hunter O. Ford, Laura C. Merrill, Jiacheng Liu, Loyal P. Murphy, and Jennifer L. Schaefer*

Department of Chemical and Biomolecular Engineering, University of Notre Dame, Notre Dame, Indiana 46556, United States

Supporting Information

ABSTRACT: Solid-state magnesium-ion conductors are desired for next-generation battery applications. Here we investigate magnesium conducting polymer electrolytes produced through dual cation exchange of a poly(ionic liquid) by mixing 1-butyl-3methylimidazolium poly[4-styrenesulfonyl(trifluoromethanesulfonyl)imide] (BMIPSTFSI) with the magnesiated analogue Mg(PSTFSI)₂. An ionic conductivity of 8.6 \times 10⁻⁵ S cm⁻¹ at 80 °C was achieved for the poly(ionic liquid), and conductivity did not significantly decrease with magnesium content up to 5 mol % Mg(PSTFSI)₂ (3.8 \times 10⁻⁵ S cm⁻¹). The characteristic poly(ionic liquid) ion-to-ion correlation peak was observable via X-ray scattering at these low magnesium contents



but disappeared at higher magnesium loadings. Polarization experiments were performed in Cu/Mg cells, resulting in sparse magnesium-rich particle-like deposits on the Cu electrode. With a lack of widespread deposition, however, either the magnesium electrodeposition or the magnesium stripping from the magnesium metal is unfavorable for this electrolyte.

KEYWORDS: polymer electrolytes, magnesium battery, polymerized ionic liquids, poly(ionic liquid)s, ionic conductivity

INTRODUCTION

With increasing demands for large-scale electrical energy storage systems, electrochemical energy storage devices with improved performance (energy density, power density, lifetime, and safety) and reduced cost are sought. 1,2 Magnesium is one of the promising alternative anode candidates for rechargeable batteries due to its widespread abundance and high theoretical volumetric capacity of 3837 mAh cm⁻³. Because of its reactivity, however, the magnesium metal surface is easily passivated by common organic solvents and magnesium salts, including organic carbonates, $Mg(ClO_4)_2$, and $Mg(BF_4)_2$, 4-7 which inhibit reversible magnesium deposition/dissolution on the surface. In an attempt to achieve reversible magnesium oxidation/reduction in conjunction with sufficient electrochemical stability, various liquid electrolytes for rechargeable Mg batteries have been investigated by using novel Mg salts or complex salt mixtures dissolved in pure ethereal solvents or ethereal containing mixtures.^{3,7–18} Recent work achieved high Coulombic efficiencies with noncorrosive electrolytes such as halogen-free salt formulations in glymes, 11,12 though many of the liquid electrolytes reported to date that support Coulombic efficiencies close to 100% are based on volatile solvents such as tetrahydrofuran or dimethoxyethane. $^{7-10}$

Solid-state electrolytes, including polymers and inorganics, have been widely studied to improve safety and high temperature performance of batteries. 19-26 While polymer electrolytes typically have lower thermal stability than

inorganic electrolytes, polymer electrolytes have the advantage of flexibility that renders greater durability to withstand the volume changes at the electrodes occurring during charge/ discharge cycling. Poly(ethylene oxide) (PEO) and related polar polymers have been a major focus for lithium polymer electrolytes, as the polar polymers bind with Li+, enable the lithium salt dissociation, and facilitate the transport of Li⁺ in the amorphous polymer matrix through segmental motion.²⁷ Polar polymers have also been investigated for multivalent polymer electrolytes. Unfortunately, dissolution of a common Mg salt such as Mg(CF₃SO₃)₂ or Mg(TFSI)₂ yields an electrolyte with a high total ionic conductivity but unacceptably low cation transference number $(t_+ \ll 0.3)^{28,29}$ It is believed that the hard Mg²⁺ cation (charge density of 540 charge nm⁻³ for Li⁺ and 1280 charge nm⁻³ for Mg²⁺ due to the effective ionic radii of 0.076 and 0.072 nm for Li⁺ and Mg²⁺, respectively)30 binds strongly to polar moieties, thereby creating effective cross-links in the polymer matrix and hindering cation transport. The only simple salt-inpolymer electrolyte reported to facilitate reversible magnesium electrodeposition and dissolution is magnesium borohydride in PEO; the conducting cation in this electrolyte is believed to be $Mg(BH_4)^+$, and it has a low oxidative stability of ~2.2 V.³⁵ Free ionic liquids and organic solvents have been added to

Received: July 2, 2019

Accepted: September 25, 2019 Published: September 25, 2019 **ACS Applied Polymer Materials**

multivalent polymer electrolytes to improve cation transport, but this results in a compromise in thermal and electrochemical stability. 34-40

Single-ion conductors, such as ionomers and polymerized ionic liquids (poly(ionic liquid)s, PILs), avoid the transport of inactive ions by bonding them to the polymer chain. The enhancement of the active ion transport number to unity mitigates the formation of concentration gradients in electrolytes during device operation, which has a number of positive impacts on performance. Lithium single-ion conducting polymer electrolytes are widely studied and promising, but the conductivities of analogous reported magnesium single-ion conductors based on PEO have very low ionic conductivities (ca. 3×10^{-5} S cm⁻¹ for Li and 2×10^{-6} S cm⁻¹ for Mg at 90 °C).

Here we report an alternative approach to prepare a magnesium conducting polymer electrolyte through dual cation exchange of a poly(ionic liquid). Previously, Forsyth and colleagues⁴² reported that the introduction of the ammonium cation in Na- and Li-based ionomers resulted in enhanced metal ion transport. As the working potential of the Mg metal anode is 660 mV higher than that of the Li metal anode (-2.38 V vs SHE in contrast with -3.04 V vs SHE), there exist many more organic cations that are electrochemically stable against Mg metal. In this work, the poly(ionic liquid) 1-butyl-3-methylimidazolium poly[4-styrenesulfonyl-(trifluoromethanesulfonyl)imide] (BMIPSTFSI) is mixed with the magnesiated analogue Mg(PSTFSI)₂ to create the dual cation exchanged polyanion as shown in Scheme 1. BMI⁺

Scheme 1. Molecular Structure of the Dual Cation Exchanged Poly(ionic liquid) Electrolyte $(Mg(PSTFSI)_2)_x(BMIPSTFSI)_{(y=100-x)}$

is chosen due to (1) enhanced charge delocalized structure and dissociability that enable higher ionic conductivity^{45,46} and (2) adequate electrochemical stability.⁴⁷ High total cation conductivities are found for these dual cation poly(ionic liquid) electrolytes with low Mg content. An electrodeposition study reveals that magnesium deposition is possible from this liquid-free electrolyte.

EXPERIMENTAL METHODS

Materials. Oxalyl chloride (Sigma-Aldrich), triethylamine (Sigma-Aldrich), 4-(dimethylamino)pyridine (DMAP, Sigma-Aldrich), anhydrous acetonitrile (Sigma-Aldrich), dimethylformamide (DMF, Sigma-Aldrich), trifluoromethylsulfonamide (TCI), dichloromethane (Sigma-Aldrich), sodium bicarbonate (NaHCO₃, Sigma-Aldrich), magnesium chloride (MgCl₂, Sigma-Aldrich), hydrochloric acid (Sigma-Aldrich), potassium carbonate (K₂CO₃, Sigma-Aldrich), dimethyl sulfoxide (DMSO, Sigma-Aldrich), tetrahydrofuran (THF, Sigma-Aldrich), and ethanol (Sigma-Aldrich) were used as purchased.

1-Butyl-3-methylimidazolium chloride (BMICl, Sigma-Aldrich) was dried under vacuum at 80 °C for 24 h before use. Sodium 4-

vinylbenzenesulfonate (Sigma-Aldrich) was dried at room temperature for 24 h under vacuum before use. Ammonium persulfate (Sigma-Aldrich) was recrystallized in deionized water before use.

Synthesis of Potassium 4-Styrenesulfonyl(trifluoromethanesulfonyl)imide (KSTFSI). KSTFSI was synthesized and polymerized by following a previously reported method.⁴⁸ Oxalyl chloride (10.0 mL) and DMF (0.435 g) were stirred in acetonitrile (200 mL) for 5 h. 4-Styrenesulfonic acid sodium salt (20 g) was added to the solution under an argon atmosphere and then stirred for a day. The resulting solution was filtered to remove sodium chloride precipitate, and then the filtrate was cooled in an ice bath. A mixture of triethylamine (40.5 mL), trifluoromethylsulfonamide (14.45 g), and DMAP (4.95 g) in acetonitrile (150 mL) was added dropwise to the filtrate solution. The mixture was then stirred for 16 h. The solvent was removed, and the resulting solid was dissolved in dichloromethane (250 mL). The solution was washed twice with 100 mL of 4% NaHCO₃(aq), followed by washing with 100 mL of 1 M hydrochloric acid. The solution was then neutralized by a solution of K₂CO₃ (27.6 g) in water (40 mL) for an hour. Finally, the product was recrystallized twice from deionized water. The successful synthesis of KSTFSI was confirmed via ¹H and ¹⁹F NMR in DMSO- d_6 .

Polymerization. KSTFSI monomer was polymerized according to a published procedure. ⁴⁸ Deionized water was purged with nitrogen gas for 24 h to deoxygenate it before use. KSTFSI (9 g) and ammonium persulfate (0.18 g) were dissolved in 180 mL of deionized water. The resulting solution was stirred at 80 °C for 1 day under nitrogen gas. The solvent was removed, and the resulting potassium poly[4-styrenesulfonyl(trifluoromethanesulfonyl)imide] (KPSTFSI) was dissolved in DMSO and precipitated with THF three times. A number-average mass (M_n) of 59100 g mol⁻¹ and a dispersity of 2.30 were determined via gel permeation chromatography.

lon Exchange with Magnesium Cation. KPSTFSI (2~g) and MgCl₂ (6~g) were dissolved in deionized water (100~mL) and stirred for 6~h. The solution was dialyzed for 4 days in deionized water in a dialysis membrane with a cutoff molecular weight of 1000~g mol⁻¹. The dialysis water was changed twice a day. Inductively coupled plasma optical emission spectrometry (ICP-OES) was used to confirm the stoichiometric exchange to the magnesiated form.

Ion Exchange with 1-Butyl-1-methylimidazolium (BMI) Cation. The KPSTFSI was exchanged to the organic cation form via a method previously reported for poly(ionic liquid) preparation. ⁴⁹ KPSTFSI (0.3 g) was stirred in acetonitrile (9 mL) overnight. BMICl (0.15 g) was dissolved in acetonitrile (2 mL) and then added into the KPSTFSI solution. The solution was stirred for 24 h. Potassium chloride (KCl) precipitate was removed with a syringe filter with a pore size of 0.4 μ m. Acetonitrile was evaporated, and then the resulting polymer was stirred in deionized water to remove KCl residue. Water was removed via filtration, and the product was further dried under vacuum at 100 °C for 24 h. Removal of potassium was confirmed via use of ICP-OES. Stoichiometric exchange of BMI was confirmed with ¹H NMR in DMSO- d_6 (Figure S1).

Mixtures. Binary mixtures of Mg(PSTFSI)₂ and BMIPSTFSI were prepared by combining the polymers in the appropriate molar ratio in an equivolume mixture of ethanol and acetonitrile and stirring for 24 h. Compositions of $(Mg(PSTFSI)_2)_x(BMIPSTFSI)_{(y=100-x)}$ are denoted as x mol % Mg(PSTFSI)₂. The solutions were cast in Teflon containers (or on a metal electrode for electrochemical measurements), and dried at room temperature in an argon-filled glovebox for a day to evaporate the bulk solvent. The samples were then further dried under vacuum at room temperature, 50 °C, 75 °C, and 100 °C for 5 h and at 120 °C for 10 h.

Nuclear Magnetic Resonance (NMR). For solution NMR measurements, ¹H and ¹⁹F NMR spectra were recorded on a Bruker Avance III HD 400 Nanobay spectrometer.

Gel Permeation Chromatography (GPC). A Waters 1515 isocratic HPLC pump with a Waters 717 autosampler, a Waters 2487 dual wavelength absorbance detector (264 nm), and a Waters 2414 refractive index detector were used to perform GPC measurements with an eluent of 0.1 M LiCl in dimethylformamide at a flow rate of

0.5 mL min⁻¹. Agilent PolarGel mixed-bed columns, composed of two PL PolarGel-M $(7.5 \times 300 \text{ mm}^2)$ and a PL PolarGel-M guard column, were maintained at 50 °C. The columns were calibrated using poly(ethylene glycol) standards. Waters Breeze v3.30 software was used to control the GPC instruments.

Differential Scanning Calorimetry (DSC). DSC experiments were performed on a DSC Q2000 (TA Instruments). Samples (5-10 mg) were sealed in aluminum pans under argon in a glovebox. The PIL-based samples underwent a heating-cooling-heating cycle from -100 to 220 °C (-50 to 280 °C for Mg(PSTFSI)₂) under nitrogen purge at 50 mL min⁻¹. The samples were first heated to 220 °C at a heating rate of 50 °C min⁻¹, then cooled to -100 °C at a cooling rate of 20 °C min⁻¹, and kept isothermal for 5 min. The second heating scan was performed by heating samples to 220 °C at a heating rate of 10 °C min⁻¹. The glass transition temperatures reported were obtained from analyzing the data from the second heating scan.

Small- and Wide-Angle X-ray Scattering (SAXS/WAXS). The samples were loaded into special glass capillary tubes with a diameter of 2 mm and sealed in an argon-filled glovebox to prevent incorporation of moisture into the samples. SAXS/WAXS measurements were obtained at the Argonne APS synchrotron beamline 12-ID-B, operated by the Chemical and Materials Science group at Argonne National Laboratory, at room temperature, and at 130 °C with an X-ray beam wavelength of 0.9322 Å (energy of 13.3 keV).

lonic Conductivity. Ionic conductivity was measured by using a broadband dielectric spectrometer with an Alpha A analyzer, outfitted with a cryostat and Quatro temperature control unit (Novocontrol Technologies, Montabaur, Germany). Samples were cast on stainless steel (SS) electrodes with glass fiber spacers with a thickness of 53 μ m. The samples were then sandwiched with another SS electrode. Coin cells were assembled and aged at 160 °C for 2 h before measurement to improve contact. Dielectric spectroscopy was measured over a frequency range of 10⁷-10⁻¹ Hz with an amplitude of 0.5 V over a temperature range from -20 to 160 °C in 20 °C intervals. Temperature was stabilized at each point for 10 min within 0.5 °C before measurement. The standard error of the conductivity measurement was <25%, and the error bars are smaller than the data points on the associated figures.

Constant Potential Test. A PARSTAT MC1000 (Princeton Applied Research) potentiostat was used to perform constant potential measurements. Polymer samples were cast on copper foil (working electrode) with a spacer with a thickness of 53 μ m. The samples were then pressed against magnesium foil. Coin cells (size 2032) were assembled, aged at 160 °C for 2 h to improve electrolyte/ electrode contact, and then aged at 80 °C for 24 h to stabilize the electrode and the electrolyte interface before the constant potential measurements. The voltage was held across the cell at -0.6 V for 24 h

Scanning Electron Microscopy (SEM) and Energy Dispersive X-ray Spectroscopy (EDS). The copper electrodes were analyzed following the potential hold with a FEI Magellan 400 at an accelerating voltage of 5 kV and current of 13 pA at a working distance of 4 mm. A Bruker energy dispersive X-ray spectrometer (EDS) was used for elemental analysis of the Cu electrode surfaces. For EDS measurements, the current was increased such that adequate signal could be achieved. Samples were sealed in a Pelco SEM pin stub vacuum desiccator in an argon-filled glovebox and then transferred to the instrument to minimize air exposure.

RESULTS AND DISCUSSION

DSC. Sample compositions and associated calorimetry data are specified in Table 1. Results of the DSC second heating scan are shown in Figure S2. The purely magnesiated polymer Mg(PSTFSI)₂ has no thermal transitions within the investigated range (up to 280 °C). Two thermal transitions are observable for the pure ionic liquid BMIPSTFSI: one at around −5 °C and the other near room temperature. The higher temperature transition increases with increasing Mg concentration for the blends. The lower temperature transition

Table 1. Polymer Compositions and Thermal Transition Data (Numbers in Parentheses Indicate Thermal Transition at Low Temperature)

$Mg(PSTFSI)_2$ concentration [x, mol %]	TFSI titrated with Mg concentration [mol %]	transition midpoint, (ionic) T_g [°C]	transition breadth, (ionic) T_g [°C]
25	40	141.8	30.4
10	18.2	87.8	16.1
5	9.5	(-5.5) 78.9	(20.1) 19.4
2.5	4.9	(-6.1) 67.7	(28.3) 9.0
0	0	(-4.9) 49.2	(24.5) 7.8

stays constant up to 5 mol % Mg(PSTFSI)₂ and is not observable for higher Mg concentrations. Two thermal transitions in poly(ionic liquid)s were previously reported by Kenji and colleagues. 50 They assigned the thermal transition at high temperature as a glass transition temperature, $T_{\rm g}$, and described that the transition at lower temperature might be due to local motions of PILs. Our samples were brittle at room temperature and softened enough at 100 °C to adhere to the surface of an aluminum pan. Thus, the thermal transition at higher temperature was assigned as the glass transition temperature. The thermal transition at lower temperature could be related to local motion of BMI⁺ and TFSI⁻, since this transition is at similar temperature regardless of Mg concentration and disappeared with higher Mg concentration where the material structure changed (as explained in the following SAXS/WAXS discussion).

The glass transition temperature as a function of composition is displayed in Figure 1 with the bars representing

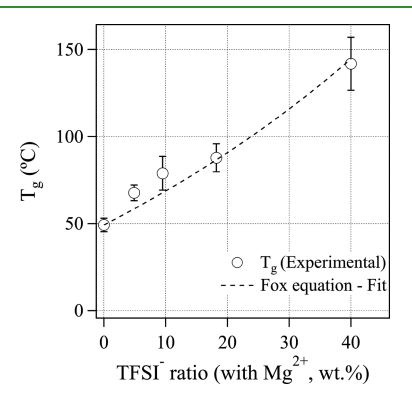


Figure 1. Glass transition temperature (T_g) vs TFSI⁻ anion ratio. The line is fit of the T_g midpoints with the Fox equation, which fails to adequately describe the data. Bars indicate the width of the glass transition.

the breadth of the transition. As expected, $T_{\rm g}$ increased with $Mg(PSTFSI)_2$ content. Also shown is the fit of the T_s midpoints to the Fox equation, which calculates the $T_{\rm g}$ of binary mixtures as⁵¹

$$\frac{1}{T_{\rm g}} = \frac{W_1}{T_{\rm g1}} + \frac{W_2}{T_{\rm g2}} \tag{1}$$

where as $T_{\rm g}$ is the glass transition of the mixture, $T_{\rm g1}$ and $T_{\rm g2}$ are the glass transitions of each component, and W_1 and W_2 are the weight fractions of each component. The Fox equation predicts the T_g of Mg(PSTFSI)₂ as 459 °C. This estimate appears too high even considering the divalency of the magnesium cation, given the reported glass transition temper**ACS Applied Polymer Materials**

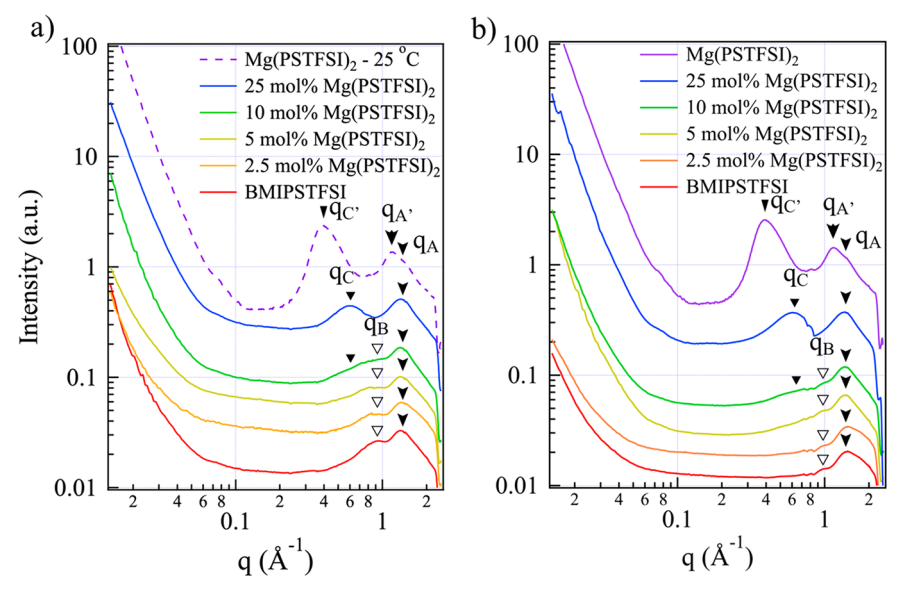


Figure 2. SAXS/WAXS of the ionic polymers at 130 $^{\circ}$ C (a) and 25 $^{\circ}$ C (b). The scattering profiles are vertically shifted to improve clarity. Mg(PSTFSI)₂ data at 25 $^{\circ}$ C was plotted as a dotted line in (a) for comparison as data at 130 $^{\circ}$ C was not available; the structure of Mg(PSTFSI)₂ is anticipated to be similar at these temperatures as the material is in the glassy state.

atures of similar polymers, such as LiPSTFSI (234 °C), NaPSTFSI (227 °C), and CsPSTFSI (197 °C). The Fox equation underestimates the $T_{\rm g}$ of the blends at low Mg content. The deviation from the Fox equation suggests additional interactions or phase segregation in the blends. 53,54

SAXS/WAXS. X-ray scattering measurements were performed to investigate the structure of the ionic polymers at 25 and 130 °C, and the corresponding data are shown in Figure 2. Structural differences are obvious between the pure BMIPSTF-SI and Mg(PSTFSI)₂, with the biggest changes in the structure of the blends occurring with 10 mol % and higher of Mg(PSTFSI)₂. Five distinct spacings are observed in the scattering profiles and are attributed to three different contributions: 55 (1) amorphous scattering from pendant-to-pendant spacing ($q_A = 1.4 \text{ Å}^{-1}$, $q_{A'} = 1.15 \text{ Å}^{-1}$), (2) ion-to-ion correlation ($q_B = 0.8 - 1.0 \text{ Å}^{-1}$), and (3) backbone-to-backbone correlation ($q_C = 0.6 \text{ Å}^{-1}$, $q_{C'} = 0.4 \text{ Å}^{-1}$). Length scales were calculated according to Bragg's law ($d = 2\pi/q$).

The amorphous scattering in the poly(ionic liquid), q_A remained at the same position ($d \approx 0.48$ nm) up to 25 mol % Mg(PSTFSI)₂ and with heating to 130 °C. Mg(PSTFSI)₂ has a dominant peak at 1.15 Å⁻¹ ($d \approx 0.55$ nm) with an inflection point at 1.4 Å⁻¹ ($d \approx 0.45$ nm), indicating that the pendant group spacing is more inhomogeneous in the magnesiated homopolymer. The intermediate peak (q_B) around 0.6–0.8 nm is related to the distance between counterions in poly(ionic liquid)s. 55 The relative intensity of this peak is increased as the material softens; at 130 $^{\circ}$ C, well above the T_{g} of BMIPSTFSI, $q_{\rm B}$ is more substantial than at room temperature which is below $T_{\rm g}$. The $q_{\rm B}$ correlation is disrupted by the magnesium doping and nearly disappears above 10 mol % Mg(PSTFSI)2. At the higher magnesium concentrations (10 mol % +), the backbone-to-backbone correlation is apparent. Backbone correlations are at similar distances for 10 and 25 mol % Mg(PSTFSI)₂ (in the range of 1.04 nm) and shifted to a larger distance (1.59 nm) for the fully magnesiated polymer. We attribute the larger backbone spacing in the Mg(PSTFSI)₂ to the lack of mixing of the polymer backbone with the ionic

phase that commonly occurs with poly(ionic liquid)s with organic cations. 55,56

Ionic Conductivity. Figure 3a displays the direct current (dc) ionic conductivity of the samples as a function of inverse

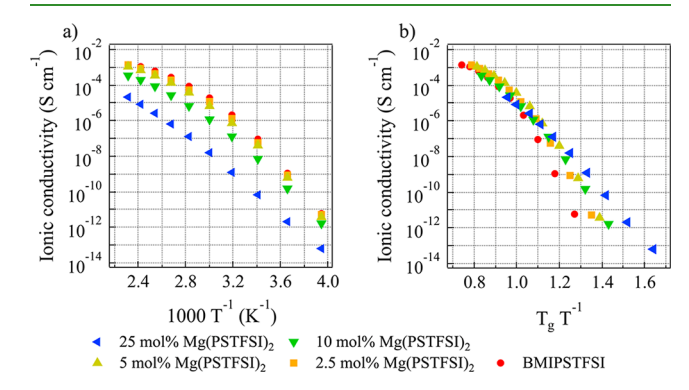


Figure 3. Ionic conductivity as a function of inverse temperature (a) and ionic conductivity as a function of normalized temperature, $T_{\rm g}/T$ (b).

temperature; the dc conductivity was not obvious within the measured frequency range for the homopolymer $\mathrm{Mg}(\mathrm{PSTFSI})_2$ as shown in Figure S3, but the values are certainly very low. As expected, the highest ionic conductivity was found for BMIPSTFSI and conductivity decreases with increasing Mg content. Only a marginal decrease in conductivity is found for up to 5 mol % Mg(PSTFSI)2, with a larger decrease at 10 mol % Mg(PSTFSI)₂ and the most significant decrease at 25 mol % Mg(PSTFSI)₂. These trends follow well with the tendency in the glass transition temperature and changes in material structure. The intensity of the backbone-to-backbone correlation $q_{\rm C}$ increases substantially from 10 to 25 mol % Mg(PSTFSI)₂ just as the conductivity significantly drops. As two BMI+ were replaced by one Mg²⁺ with increasing Mg content, the cation-anion interactions became stronger due to the lack of low charge density of BMI+ and the high charge density of Mg²⁺. The larger organic cation can act as a plasticizer, improving the segmental motion of polymer chain compared to a higher charge density cation. To investigate the relationship between segmental motion and ionic conductivity, dc ionic conductivity was plotted against temperature normalized by the glass transition temperature (Figure 3b). The ionic conductivity of all compositions are similar to each other above the glass transition temperature $(T_{\rm g}/T < 1)$, indicating that the ion transport is coupled to polymer chain segmental motion.

Unfortunately, we are unable to tell from the ionic conductivity data what portion of the conductivity is due to Mg transport as opposed to BMI transport. Mg electro-deposition will be discussed in the following section. The Mg transference number $(t_{\rm Mg}^{2*})$ could not be directly measured by the three step (impedance–polarization–impedance) method commonly used for lithium systems due to the high overpotential of Mg electrodeposition/dissolution, where the method is not applicable. In addition, neither of the Mg isotopes is amenable to pulsed-field-gradient nuclear magnetic resonance spectroscopy (PFG-NMR), a technique commonly applied to measure $^7{\rm Li}$, $^1{\rm H}$, and $^{19}{\rm F}$ self-diffusion coefficients from which a transference number can be inferred.

Electrodeposition of Magnesium. To investigate Mg long-range transport and electrodeposition, a constant voltage of -0.6~V was applied to a Cu/5 mol % Mg(PSTFSI)₂/Mg cell at 80 °C. The current response of this cell is displayed in Figure 4 and Figure S4. The polarization current dropped

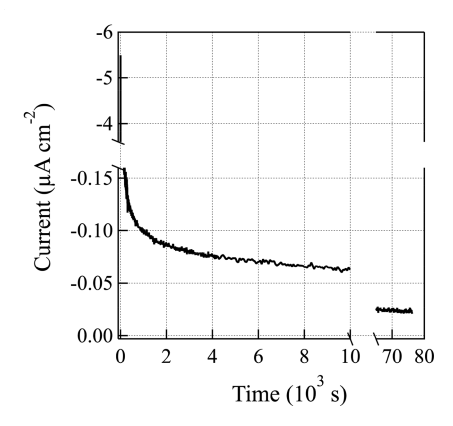


Figure 4. Constant voltage polarization test at 80 °C and -0.6 V. Split of *y*-axis shows the difference in scale between the initial current and the steady-state current. Split of *x*-axis shows the difference in scale between the current at 10,000 s and the steady-state current at the end of measurement. The figure without the split axes is shown in Figure S4.

rapidly at the start and then stabilized over time. Initially, all the mobile charge carriers respond to the electric field. At long times, the current is due to charge carriers with a source and drain undergoing reduction/oxidation (here, magnesium electrodissolution/electrodeposition) or decomposition of the electrolyte. The ratio of initial current density ($i_0 = 5.49~\mu A$ cm⁻²) and steady-state current density after 20 h ($i_{ss} = 2.30 \times 10^{-2}~\mu A$ cm⁻²), i_{ss}/i_0 , was calculated as 0.00042. Because the BMI⁺ cation is larger and its charge is more delocalized than Mg²⁺, transport of BMI⁺ is easier than Mg²⁺. The large initial current drop suggests that a higher proportion of the initial current is due to BMI⁺ transport. Because the absolute magnitude of the steady-state current is small, the source could be oxidation/reduction of magnesium, decomposition, or both.

To interrogate the possible deposition of magnesium, the copper electrode surface was analyzed by SEM-EDS after the polarization test. We found that the copper electrode was mostly clean, with sporadic particles. Figure 5 displays a

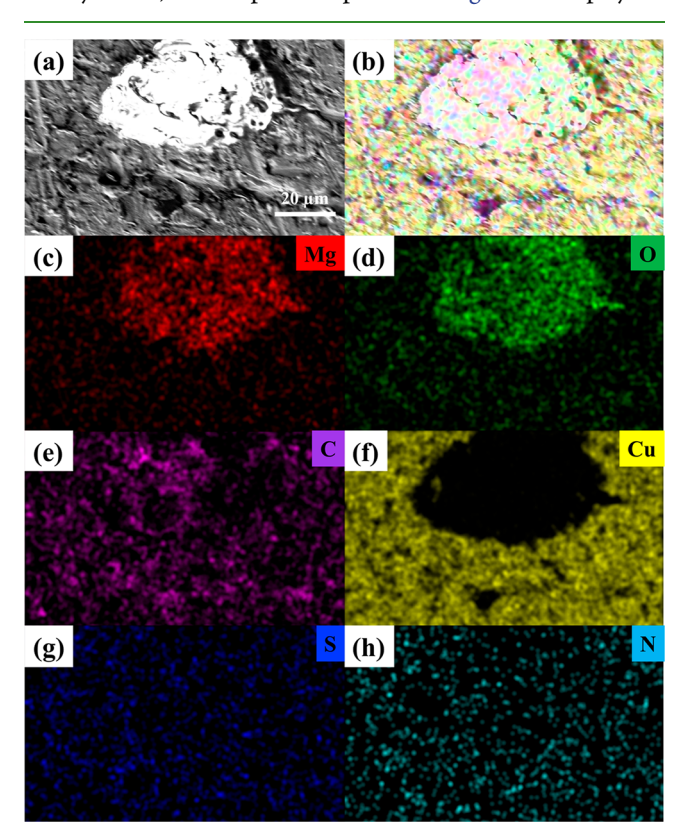


Figure 5. SEM image of copper electrode surface after polarization test at 80 °C (a) and corresponding EDS elemental mapping (b-h).

particle with a diameter of around 20 μ m with high Mg and oxygen content and low carbon, sulfur, and nitrogen content. The Cu electrode before the polarization test is shown in Figure S5 for comparison. Some oxidation is expected due to the transfer when loading the sample in the SEM, but less than observed here. Other particle deposits (see Figure S6) had higher proportions of magnesium compared with oxygen and carbon. Thus, we can conclude that transport of Mg²⁺ and electrodeposition of Mg is possible from the dual cation exchanged poly(ionic liquid). As metallic Mg was used as the counter electrode and magnesium source, it may be that the electrodissolution of Mg is not favorable and therefore limits the extent of Mg deposition.

CONCLUSION

Dual cation exchanged poly(ionic liquid)s were investigated as electrolytes for magnesium batteries. It was found that introduction of Mg(PSTFSI)₂ into BMIPSTFSI results in relatively small changes to the ionic conductivity, thermal properties, and structural properties at low loadings (<10 mol % Mg(PSTFSI)₂). Polarization experiments were performed in asymmetric coin cells to probe the possibility of magnesium deposition from the poly(ionic liquid) electrolyte. Magnesium-rich particle-like deposits were observed on copper, confirming that the electrodeposition is indeed possible. However, lack of widespread and uniform magnesium deposition coupled with the low steady-state current during polarization indicates that

either the magnesium stripping from the counter electrode or the magnesium electrodeposition process is unfavorable.

ASSOCIATED CONTENT

S Supporting Information

The Supporting Information is available free of charge on the ACS Publications website at DOI: 10.1021/acsapm.9b00614.

¹H NMR of BMIPSTFSI, DSC curves, dielectric spectroscopy data for Mg(PSTFSI)₂, polarization curve, supplementary SEM-EDS (PDF)

AUTHOR INFORMATION

Corresponding Author

*E-mail: Jennifer.L.Schaefer.43@nd.edu.

ORCID ®

Jennifer L. Schaefer: 0000-0003-4293-6328

Notes

The authors declare no competing financial interest.

■ ACKNOWLEDGMENTS

We thank Dr. Xiaobing Zuo from Argonne National Laboratory for assistance in collecting SAXS spectra, Dr. Phillip D. Pickett and the National Institute of Standards and Technology for GPC measurements, Prof. Ruilan Guo for DSC instrumentation, Jon Loftus and the Notre Dame Center for Environmental Science and Technology for ICP-OES instrumentation, and Tatyana Orlova and the University of Notre Dame Integrated Imaging Facilities for SEM. This research used resources of the Advanced Photon Source, a U.S. Department of Energy (DOE) Office of Science User Facility operated for the DOE Office of Science by Argonne National Laboratory under Contract DE-AC02-06CH11357. The authors gratefully acknowledge funding from the National Science Foundation via Award DMR-1654162.

REFERENCES

- (1) Dunn, B.; Kamath, H.; Tarascon, J.-M. Electrical Energy Storage for the Grid: A Battery of Choices. *Science* **2011**, 334 (6058), 928–935
- (2) Landry, M.; Gagnon, Y. Energy Storage: Technology Applications and Policy Options. *Energy Procedia* 2015, 79, 315–320.
- (3) Muldoon, J.; Bucur, C. B.; Oliver, A. G.; Sugimoto, T.; Matsui, M.; Kim, H. S.; Allred, G. D.; Zajicek, J.; Kotani, Y. Electrolyte Roadblocks to a Magnesium Rechargeable Battery. *Energy Environ. Sci.* **2012**, *5* (3), 5941–5950.
- (4) Aurbach, D.; Gofer, Y.; Schechter, A.; Chusid, O.; Gizbar, H.; Cohen, Y.; Moshkovich, M.; Turgeman, R. A Comparison between the Electrochemical Behaviour of Reversible Li and Mg Electrodes. *J. Power Sources* **2001**, *97*–*98*, 269–273.
- (5) Lu, Z.; Schechter, A.; Moshkovich, M.; Aurbach, D. On the Electrochemical Behavior of Magnesium Electrodes in Polar Aprotic Electrolyte Solutions. *J. Electroanal. Chem.* **1999**, 466 (2), 203–217.
- (6) Amir, N.; Vestfrid, Y.; Chusid, O.; Gofer, Y.; Aurbach, D. Progress in Nonaqueous Magnesium Electrochemistry. *J. Power Sources* **2007**, 174 (2), 1234–1240.
- (7) Attias, R.; Salama, M.; Hirsch, B.; Goffer, Y.; Aurbach, D. Anode-Electrolyte Interfaces in Secondary Magnesium Batteries. *Joule* **2019**, 3 (1), 27–52.
- (8) Zhao-Karger, Z.; Fichtner, M. Magnesium—Sulfur Battery: Its Beginning and Recent Progress. MRS Commun. 2017, 7 (04), 770—784
- (9) Zhao-Karger, Z.; Liu, R.; Dai, W.; Li, Z.; Diemant, T.; Vinayan, B. P.; Bonatto Minella, C.; Yu, X.; Manthiram, A.; Behm, R. J.; Ruben, M.; Fichtner, M. Toward Highly Reversible Magnesium—Sulfur

- Batteries with Efficient and Practical Mg[B(Hfip)4]2 Electrolyte. ACS Energy Lett. 2018, 3 (8), 2005–2013.
- (10) Zhao-Karger, Z.; Gil Bardaji, M. E.; Fuhr, O.; Fichtner, M. A New Class of Non-Corrosive, Highly Efficient Electrolytes for Rechargeable Magnesium Batteries. *J. Mater. Chem. A* **2017**, 5 (22), 10815–10820.
- (11) Tutusaus, O.; Mohtadi, R.; Arthur, T. S.; Mizuno, F.; Nelson, E. G.; Sevryugina, Y. V. An Efficient Halogen-Free Electrolyte for Use in Rechargeable Magnesium Batteries. *Angew. Chem., Int. Ed.* **2015**, *54* (27), 7900–7904.
- (12) Luo, J.; Bi, Y.; Zhang, L.; Zhang, X.; Liu, T. L. A Stable, Non-Corrosive Perfluorinated Pinacolatoborate Mg Electrolyte for Rechargeable Mg Batteries. *Angew. Chem., Int. Ed.* **2019**, 58 (21), 6967–6971.
- (13) Gregory, T. D.; Hoffman, R. J.; Winterton, R. C. Nonaqueous Electrochemistry of Magnesium: Applications to Energy Storage. *J. Electrochem. Soc.* **1990**, *137* (3), *775*–780.
- (14) Aurbach, D.; Cohen, Y.; Moshkovich, M. The Study of Reversible Magnesium Deposition by In Situ Scanning Tunneling Microscopy. *Electrochem. Solid-State Lett.* **2001**, 4 (8), A113–A116.
- (15) Merrill, L. C.; Schaefer, J. L. Electrochemical Properties and Speciation in Mg(HMDS)2-Based Electrolytes for Magnesium Batteries as a Function of Ethereal Solvent Type and Temperature. *Langmuir* 2017, 33 (37), 9426–9433.
- (16) Merrill, L. C.; Schaefer, J. L. Conditioning-Free Electrolytes for Magnesium Batteries Using Sufone—Ether Mixtures with Increased Thermal Stability. *Chem. Mater.* **2018**, *30* (12), 3971–3974.
- (17) Merrill, L. C.; Schaefer, J. L. The Influence of Interfacial Chemistry on Magnesium Electrodeposition in Non-Nucleophilic Electrolytes Using Sulfone-Ether Mixtures. *Front. Chem.* **2019**, *7*, 194.
- (18) Zhao-Karger, Z.; Zhao, X.; Fuhr, O.; Fichtner, M. Bisamide Based Non-Nucleophilic Electrolytes for Rechargeable Magnesium Batteries. *RSC Adv.* **2013**, 3 (37), 16330–16335.
- (19) Xu, K. Electrolytes and Interphases in Li-Ion Batteries and Beyond. Chem. Rev. 2014, 114, 11503-11618.
- (20) Rajput, N. N.; Seguin, T. J.; Wood, B. M.; Qu, X.; Persson, K. A. Elucidating Solvation Structures for Rational Design of Multivalent Electrolytes—A Review. *Top. Curr. Chem.* **2018**, *376* (3), 19.
- (21) Polu, A. R.; Kumar, R.; Rhee, H. W. Magnesium Ion Conducting Solid Polymer Blend Electrolyte Based on Biodegradable Polymers and Application in Solid-State Batteries. *Ionics* **2015**, *21* (1), 125–132.
- (22) Park, B.; Lee, C. H.; Xia, C.; Jung, C. Characterization of Gel Polymer Electrolyte for Suppressing Deterioration of Cathode Electrodes of Li Ion Batteries on High-Rate Cycling at Elevated Temperature. *Electrochim. Acta* **2016**, *188*, 78–84.
- (23) Thangadurai, V.; Narayanan, S.; Pinzaru, D. Garnet-Type Solid-State Fast Li Ion Conductors for Li Batteries: Critical Review. *Chem. Soc. Rev.* **2014**, *43* (13), 4714–4727.
- (24) Mindemark, J.; Lacey, M. J.; Bowden, T.; Brandell, D. Beyond PEO—Alternative Host Materials for Li+-Conducting Solid Polymer Electrolytes. *Prog. Polym. Sci.* **2018**, *81*, 114–143.
- (25) Sai Gautam, G.; Canepa, P.; Urban, A.; Bo, S.-H.; Ceder, G. Influence of Inversion on Mg Mobility and Electrochemistry in Spinels. *Chem. Mater.* **2017**, *29* (18), 7918–7930.
- (26) Wang, L.-P.; Zhao-Karger, Z.; Klein, F.; Chable, J.; Braun, T.; Schür, A. R.; Wang, C.-R.; Guo, Y.-G.; Fichtner, M. MgSc2Se4—A Magnesium Solid Ionic Conductor for All-Solid-State Mg Batteries? *ChemSusChem* **2019**, *12* (10), 2286–2293.
- (27) Meyer, W. H. Polymer Electrolytes for Lithium-Ion Batteries. *Adv. Mater.* **1998**, *10* (6), 439–448.
- (28) Pandey, G. P.; Hashmi, S. A. Experimental Investigations of an Ionic-Liquid-Based, Magnesium Ion Conducting, Polymer Gel Electrolyte. *J. Power Sources* **2009**, *187* (2), *627*–*634*.
- (29) Kumar, Y.; Hashmi, S. A.; Pandey, G. P. Ionic Liquid Mediated Magnesium Ion Conduction in Poly(Ethylene Oxide) Based Polymer Electrolyte. *Electrochim. Acta* **2011**, *56* (11), 3864–3873.

- (30) Shannon, R. D. Revised Effective Ionic Radii and Systematic Studies of Interatomic Distances in Halides and Chalcogenides. *Acta Cryst.* **1976**, 32 (5), 751–767.
- (31) Borodin, O.; Smith, G. D. Mechanism of Ion Transport in Amorphous Poly(Ethylene Oxide)/LiTFSI from Molecular Dynamics Simulations. *Macromolecules* **2006**, 39 (4), 1620–1629.
- (32) Bakker, A.; Gejji, S.; Lindgren, J.; Hermansson, K.; Probst, M. M. Contact Ion Pair Formation and Ether Oxygen Coordination in the Polymer Electrolytes M[N(CF3SO2)2]2PEOn for M=Mg, Ca, Sr and Ba. *Polymer* **1995**, 36 (23), 4371–4378.
- (33) Shao, Y.; Rajput, N. N.; Hu, J.; Hu, M.; Liu, T.; Wei, Z.; Gu, M.; Deng, X.; Xu, S.; Han, K. S.; Wang, J.; Nie, Z.; Li, G.; Zavadil, K. R.; Xiao, J.; Wang, C.; Henderson, W. A.; Zhang, J.-G.; Wang, Y.; Mueller, K. T.; Persson, K.; Liu, J. Nanocomposite Polymer Electrolyte for Rechargeable Magnesium Batteries. *Nano Energy* 2015, 12, 750–759.
- (34) Saha, P.; Datta, M. K.; Velikokhatnyi, O. I.; Manivannan, A.; Alman, D.; Kumta, P. N. Rechargeable Magnesium Battery: Current Status and Key Challenges for the Future. *Prog. Mater. Sci.* **2014**, *66*, 1–86
- (35) Mitra, S.; Shukla, A. K.; Sampath, S. Electrochemical Capacitors with Plasticized Gel-Polymer Electrolytes. *J. Power Sources* **2001**, *101* (2), 213–218.
- (36) Asmara, S. N.; Kufian, M. Z.; Majid, S. R.; Arof, A. K. Preparation and Characterization of Magnesium Ion Gel Polymer Electrolytes for Application in Electrical Double Layer Capacitors. *Electrochim. Acta* **2011**, *57*, 91–97.
- (37) Tang, X.; Muchakayala, R.; Song, S.; Zhang, Z.; Polu, A. R. A Study of Structural, Electrical and Electrochemical Properties of PVdF-HFP Gel Polymer Electrolyte Films for Magnesium Ion Battery Applications. *J. Ind. Eng. Chem.* **2016**, *37*, 67–74.
- (38) Pandey, G. P.; Kumar, Y.; Hashmi, S. A. Ionic Liquid Incorporated PEO Based Polymer Electrolyte for Electrical Double Layer Capacitors: A Comparative Study with Lithium and Magnesium Systems. *Solid State Ionics* **2011**, *190* (1), 93–98.
- (39) Ikeda, S.; Mori, Y.; Furuhashi, Y.; Masuda, H. Multivalent Cation Conductive Solid Polymer Electrolytes Using Photo-Cross-Linked Polymers: II. Magnesium and Zinc Trifluoromethanesulfonate Systems. *Solid State Ionics* **1999**, *121* (1), 329–333.
- (40) Sarangika, H. N. M.; Dissanayake, M. A. K. L.; Senadeera, G. K. R.; Rathnayake, R. R. D. V; Pitawala, H. M. J. C. Polyethylene Oxide and Ionic Liquid-Based Solid Polymer Electrolyte for Rechargeable Magnesium Batteries. *Ionics* **2017**, 23 (10), 2829–2835.
- (41) Qian, W.; Texter, J.; Yan, F. Frontiers in Poly(Ionic Liquid)s: Syntheses and Applications. *Chem. Soc. Rev.* **2017**, 46 (4), 1124–1159
- (42) Li, J.; Zhu, H.; Wang, X.; MacFarlane, D. R.; Armand, M.; Forsyth, M. Increased Ion Conduction in Dual Cation [Sodium] [Tetraalkylammonium] Poly[4-Styrenesulfonyl-(Trifluoromethylsulfonyl)Imide-Co-Ethylacrylate] Ionomers. J. Mater. Chem. A 2015, 3 (39), 19989—19995.
- (43) Ford, H. O.; Merrill, L. C.; He, P.; Upadhyay, S. P.; Schaefer, J. L. Cross-Linked Ionomer Gel Separators for Polysulfide Shuttle Mitigation in Magnesium-Sulfur Batteries: Elucidation of Structure-Property Relationships. *Macromolecules* **2018**, *51* (21), 8629–8636.
- (44) Thelen, J. L.; Inceoglu, S.; Venkatesan, N. R.; Mackay, N. G.; Balsara, N. P. Relationship between Ion Dissociation, Melt Morphology, and Electrochemical Performance of Lithium and Magnesium Single-Ion Conducting Block Copolymers. *Macromolecules* 2016, 49 (23), 9139–9147.
- (45) Ohno, H. Physical Properties of Ionic Liquids for Electrochemical Applications. *Electrodeposition from Ionic Liquids* **2017**, 55–94.
- (46) Fernandes, A. M.; Rocha, M. A. A.; Freire, M. G.; Marrucho, I. M.; Coutinho, J. A. P.; Santos, L. M. N. B. F. Evaluation of Cation-Anion Interaction Strength in Ionic Liquids. *J. Phys. Chem. B* **2011**, *115* (14), 4033–4041.

- (47) Lewandowski, A.; Swiderska-Mocek, A. Lithium-Metal Potential in Li+ Containing Ionic Liquids. *J. Appl. Electrochem.* **2010**, 40 (3), 515–524.
- (48) Meziane, R.; Bonnet, J. P.; Courty, M.; Djellab, K.; Armand, M. Single-Ion Polymer Electrolytes Based on a Delocalized Polyanion for Lithium Batteries. *Electrochim. Acta* **2011**, *57* (1), 14–19.
- (49) Shaplov, A. S.; Vlasov, P. S.; Armand, M.; Lozinskaya, E. I.; Ponkratov, D. O.; Malyshkina, I. A.; Vidal, F.; Okatova, O. V.; Pavlov, G. M.; Wandrey, C.; Godovikov, I. A.; Vygodskii, Y. S. Design and Synthesis of New Anionic "Polymeric Ionic Liquids" with High Charge Delocalization. *Polym. Chem.* **2011**, 2 (11), 2609–2618.
- (50) Nakamura, K.; Saiwaki, T.; Fukao, K. Dielectric Relaxation Behavior of Polymerized Ionic Liquid. *Macromolecules* **2010**, 43 (14), 6092–6098.
- (51) Fox, G. T. Influence of Diluent and of Copolymer Composition on the Glass Temperature of a Poly-Mer System. *Bull. Am. Phys. Soc.* 1956. 1, 123
- (52) Stacy, E. W.; Gainaru, C. P.; Gobet, M.; Wojnarowska, Z.; Bocharova, V.; Greenbaum, S. G.; Sokolov, A. P. Fundamental Limitations of Ionic Conductivity in Polymerized Ionic Liquids. *Macromolecules* **2018**, *51* (21), 8637–8645.
- (53) Brostow, W.; Chiu, R.; Kalogeras, I. M.; Vassilikou-Dova, A. Prediction of Glass Transition Temperatures: Binary Blends and Copolymers. *Mater. Lett.* **2008**, *62* (17), 3152–3155.
- (54) Tiyapiboonchaiya, C.; MacFarlane, D. R.; Sun, J.; Forsyth, M. Polymer-in-Ionic-Liquid Electrolytes. *Macromol. Chem. Phys.* **2002**, 203 (13), 1906–1911.
- (55) la Cruz, D. S.; Green, M. D.; Ye, Y.; Elabd, Y. A.; Long, T. E.; Winey, K. I. Correlating Backbone-to-Backbone Distance to Ionic Conductivity in Amorphous Polymerized Ionic Liquids. *J. Polym. Sci., Part B: Polym. Phys.* **2012**, *50* (5), 338–346.
- (56) Liu, H.; Paddison, S. J. Direct Comparison of Atomistic Molecular Dynamics Simulations and X-Ray Scattering of Polymerized Ionic Liquids. *ACS Macro Lett.* **2016**, 5 (4), 537–543.
- (57) Tudryn, G. J.; Liu, W.; Wang, S. W.; Colby, R. H. Counterion Dynamics in Polyester-Sulfonate Ionomers with Ionic Liquid Counterions. *Macromolecules* **2011**, *44* (9), 3572–3582.
- (58) Bruce, P. G.; Vincent, C. A. Steady State Current Flow in Solid Binary Electrolyte Cells. *J. Electroanal. Chem. Interfacial Electrochem.* 1987, 225 (1), 1–17.